ISSN 1063-7788, Physics of Atomic Nuclei, 2020, Vol. 83, No. 2, pp. 252–257. © Pleiades Publishing, Ltd., 2020.

ELEMENTARY PARTICLES AND FIELDS
Experiment

The Anticoincidence System of Space-Based Gamma-Ray Telescope GAMMA-400, Test Beam Studies of Anticoincidence Detector Prototype with SiPM Readout

A. I. Arkhangelskiy[1),2)*], A. M. Galper[1),2)], I. V. Arkhangelskaja[2)], A. V. Bakaldin[3)], I. V. Chernysheva[2)], O. D. Dalkarov[1)], A. E. Egorov[1)], Yu. V. Gusakov[1)], M. D. Kheymits[2)], A. A. Leonov[1),2)], N. Yu. Pappe[1)], M. F. Runtso[2)], Yu. I. Stozhkov[1)], S. I. Suchkov[1)], N. P. Topchiev[1)], and Yu. T. Yurkin[2)]

Received July 11, 2019; revised July 11, 2019; accepted July 11, 2019

Abstract—The GAMMA-400 gamma-ray telescope is planned for the launch at the end of 2026 on the Navigator service platform designed by Lavochkin Association on an elliptical orbit with following initial parameters: an apogee ∼300 000, a perigee ∼500 km, a rotation period ∼7 days and inclination of 51.4°. The apparatus is expected to operate for more than 5 years, reaching an unprecedented sensitivity for the search of dark matter signatures and the study of the unresolved and so far unidentified gamma-ray sources. The segmented anticoincidence counters surround the converter-tracker and calorimeter of the telescope with the purpose of vetoing to assure a clean track reconstruction and charged particle background suppression. The anticoincidence detector prototype based on long BC-408 scintillator with silicon photomultipliers readout was tested using 300-MeV positron beam of synchrotron C-25P "PAKHRA" of Lebedev Physical Institute. The measurement setup, design concepts for the prototype detector together with test results are discussed.

DOI: 10.1134/S1063778820020039

1. INTRODUCTION

The scientific project GAMMA-400 [1, 2] is one of the new generation of space observatories intended for an indirect search for signatures of dark matter in the cosmic-ray fluxes, precision investigation of the characteristics of diffuse gamma-ray emission and gamma-rays from the Sun during periods of solar activity, gamma-ray bursts, extended and point gamma-ray sources in the wide energy range from several tens of MeV up to the TeV region, electron/positron and cosmic-ray nuclei fluxes with energies up to $\sim 10^{15}$ eV by means of the GAMMA-400 gamma-ray telescope that represents the core of the scientific complex, installed on the Navigator service platform [3] designed by Lavochkin Association. For gamma rays with the energy ∼100 GeV the expected energy and angular resolution are ∼2% and ∼0.01° respectively and the electron/proton rejection factor is $\sim 5 \times 10^5$. In Fig. 1 the physical model of the gamma-ray telescope is presented. The C designates the converter-tracker consisting of 13 layers of double (x, y) tracking coordinate detectors with total thickness about $1X_0$ (radiation length). The first 11 layers are interleaved with tungsten conversion foils (first 7 layers of $0.1X_0$ and next 4 layers of $0.025X_0$). The last two layers have no tungsten. The data from the converter-tracker is used for high precision determination of the gamma-quanta conversion point and reconstruction of the trajectory of the primary and secondary charged particles. The ACS is segmented anticoincidence system (135 scintillator strips) which includes one top detector $\mathrm{AC}_{\mathrm{top}}$ and four lateral detectors $\mathrm{AC1}_{\mathrm{lat}}$–$\mathrm{AC4}_{\mathrm{lat}}$ surrounding convertor-tracker for discrimination between incoming charged particles and gamma-quanta with an efficiency of $\geqslant$99.95%. All anticoincidence counters, as well as LD, $S3$, and $S4$ are made of two oriented in parallel layers of 1-cm thickness, 10-cm width BC-408 polyvinyltoluene scintillator strips with different length. The strips of one layer are displaced with respect to the strips of the other layer so that there are no rectilinear slits in the system. The TOFS—time-of-flight system, consists of hodoscope of four oriented perpendicularly layers of 1-cm thickness, 10-

[1)]Lebedev Physical Institute, Russian Academy of Sciences, Moscow, Russia.
[2)]National Research Nuclear University MEPhI (Moscow Engineering Physics Institute), Moscow, Russia.
[3)]Scientific Research Institute of System Analysis, Russian Academy of Sciences, Moscow, Russia.
[*]E-mail: AIArkhangelskij@mephi.ru

cm width, 100-cm (top) and 80-cm (bottom) length BC-408 plastic scintillation counters combined in two detector planes $S1$ and $S2$ located at the distance of 50 cm between the convertor-tracker C and calorimeter CC. The TOFS provides a fast trigger to gamma-ray telescope readout electronics by measuring the particles charge, crossing time and position, and separates upward from downward going particles within 10^{-3} level. The CC is an 80×80 cm^2, $\sim 16X_0$ thick coordinate-sensitive calorimeter to measure the incoming particles energy with resolution of $\sim 2\%$ for gamma-rays with $E_\gamma \geqslant 100$ GeV and separate $e^\pm$ and photons from hadrons at $\sim 5 \times 10^{-5}$ level. The CC includes preshower CC1 (consists of two CsI(Tl) planes with total thickness of $\sim 2X_0$, two layers of double (x, y) tracking coordinate detectors and fast plastic scintillation detector $S3$), the total-absorption calorimeter CC2, based on the set of CsI(Tl) crystals $\sim 16X_0$ thick, the anticoincidence LD and leakage $S4$ plastic detectors. Four fast plastic detectors ACS, TOFS, $S3$ and $S4$ are included in fast trigger logic in the main telescope aperture.

The space-based gamma-ray telescope must effectively separate photons from charged particles of instrumental background and cosmic rays. The anticoincidence system (ACS) of gamma-ray telescopes is suffered from the self-veto (backsplash) effect when the products of the high-energy photon interactions in the instrument's calorimeter, mainly low-energy electromagnetic shower particles moving in the direction opposite to the direction of the detected photons, cause a veto signal in the ACS, resulting in the degradation of the efficiency for high-energy (>5 GeV) gamma rays. One method of this self-veto effect reduction is segmenting the ACS into tiles and vetoing an event only if the pulse appears in the tile through which the reconstructed event trajectory passes [4]. Further improvement is time-based backsplash rejection technique [5] based on ignoring the veto signals in appropriate segments of ACS within the time interval in which backsplash particles hit the ACS. This time interval start moment and duration depend on the detector geometry and for the GAMMA-400 telescope averages out from 3 ns to 12 ns after TOFS triggering. It requires the intrinsic time resolution of TOFS and ACS segments better than 500 ps for effective self-vetoing suppression. In this case the proton impurity in the selected gamma rays and the loss of useful events do not exceed 10^{-5} and 10% respectively [6].

2. EXPERIMENTAL SETUP

The tested detector presents two strips of polyvinyltoluene scintillator BC-408 with dimensions of $1280 \times 100 \times 10$ mm^3, wrapped with one layer of Tyvek

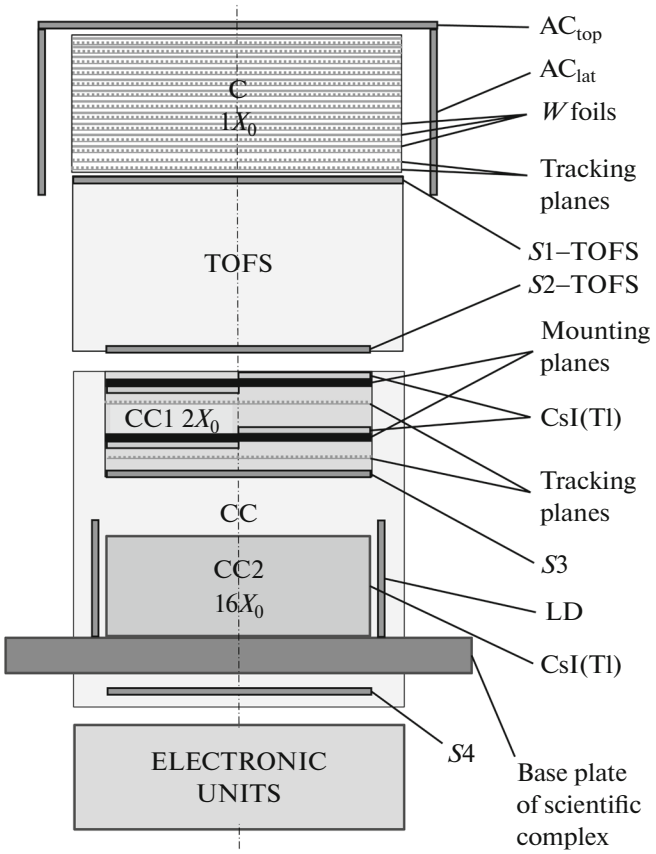

Fig. 1. Sketch of the GAMMA-400 gammaray telescope.

reflective material and placed into 1.5-mm thick aluminum cover. At the middle of each strip the FC-type fiber optic adapters are situated for optic cables' connection from laser monitoring system. Each strip is viewed at the opposite shortest ends by two photo-sensor blocks which consist of four 6×6 mm^2 silicon photomultipliers (SiPM) of the type SensL MicroFC-60035-SMT [7] connected in parallel and frontend electronics. Only "slow" SiPM outputs were used in this prototype variant. The amplified and shaped signals from both sides of the detector are split into two paths: the first signal goes directly to the LeCroy WaveRunner 6Zi digital oscilloscope, for amplitude and charge analysis, and the second signal goes through the constant fraction discriminator (CFD) ORTEC Model 935 for timing analysis. Threshold of CFD was set at about 25% of the most probable energy deposited by minimum-ionizing particles crossing the whole thickness of the scintillator (10 mm). The bias voltage for SiPMs was set at 29.5 V level (~5 V above SiPM breakdown voltage).

The primary beam of the synchrotron C-25P "PAKHRA" of Lebedev Physical Institute consists

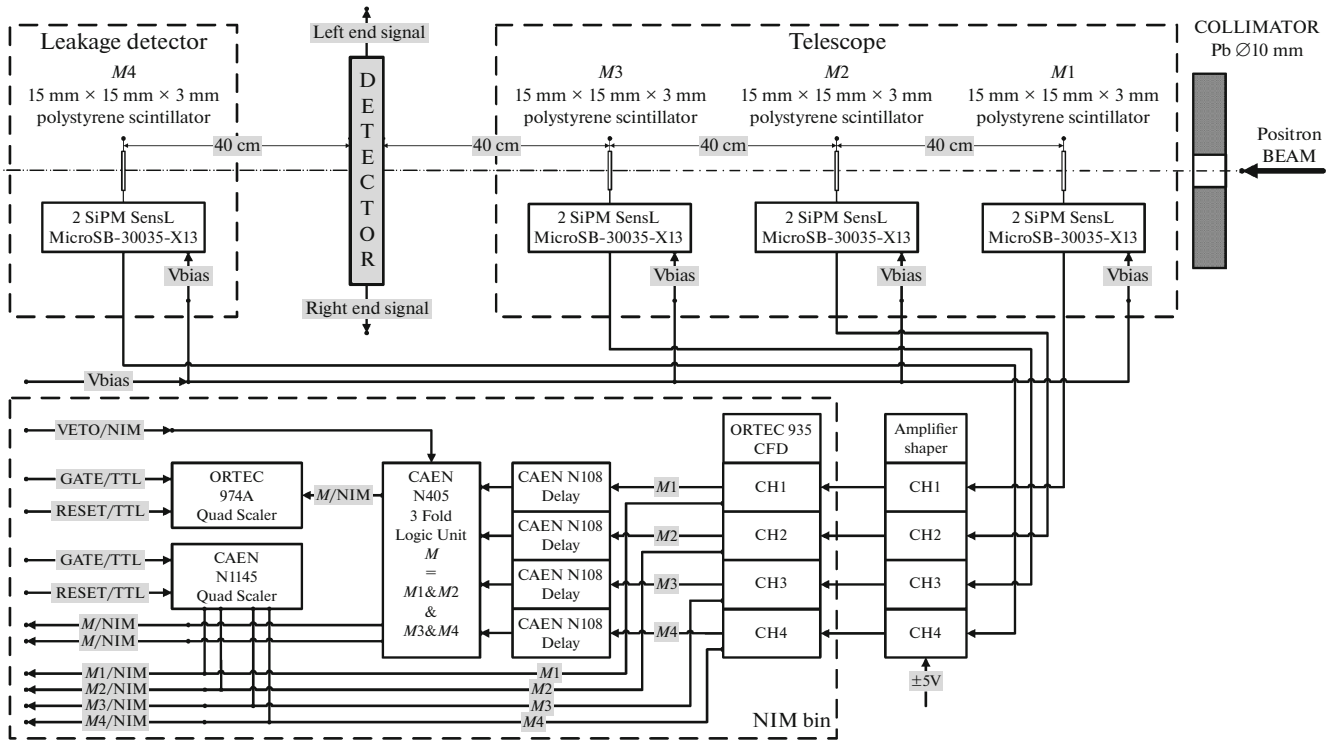

Fig. 2. The functional diagram of experimental setup. The dash–dotted line represents the positron beam line. The NIM and TTL signatures mark type of logical signals.

of 300–850 MeV electrons with particle intensity up to 2×10^{12} s^{-1} and repetition frequency of 50 Hz. Bremsstrahlung photon beam is formed by the interaction of accelerated electrons with an internal tungsten target with a thickness of $0.22X_0$ (X_0—radiation length) placed inside the accelerator vacuum chamber. This beam is used to create a secondary positron beam by $e\pm$ pair production on copper converter with 0.1–5 mm thickness. Secondary positrons with particle momentum of 300 MeV/c and intensity up to $\sim$100 s^{-1} cm^{-2} are selected using dipole magnet. The studied detector was installed on a remote controlling platform which allows horizontally and vertically moves of the detector with respect to the beam position in the range of $\pm$40 cm with the accuracy of 1 mm. A beam monitor for secondary positrons' selection installed behind the 10-mm diameter lead collimator consists of four $15 \times 15 \times 3$ mm^3 polystyrene (IHEP_SC-301) scintillation counters $M1$-$M4$ wrapped with aluminized mylar film and coupled with silicon grease BC-630 from one side with two 3×3 mm^2 SensL MicroSB-30035-X13 SiPMs connected in parallel. These counters are installed on high-precision horizontal and vertical slide positioners for finely positioning of the monitor counters with respect to the positron beam (range $\pm$6.5 mm with 10-μm accuracy). The signals from each SiPM pair are amplified by two-stage broad-band shaper-amplifiers with pole-zero cancellation circuits based on fast AD8000 operational amplifiers, produced output signals with rise-time of $\sim$3.5 ns and width of $T_{90} \sim 10$ ns. The

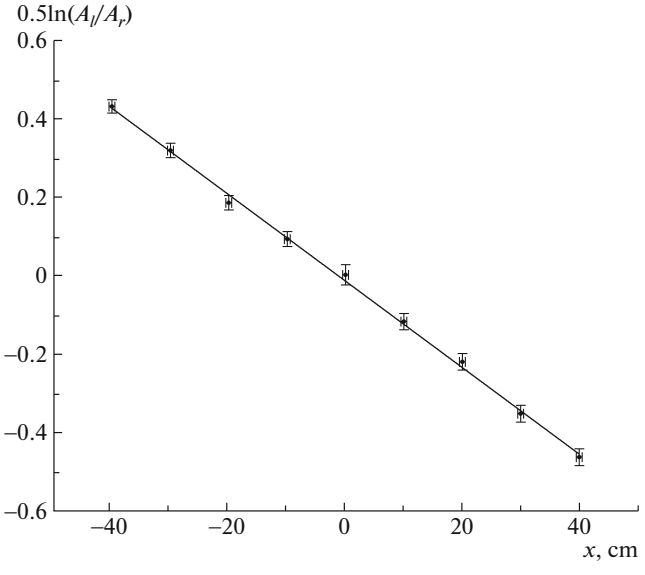

Fig. 3. Logarithmic ratio of amplitude of signals from the left and right ends of prototype detector. The inverse slope of the linear fit indicates the attenuation length $\lambda = 91 \pm 1$ cm of scintillation light in the scintillator strip.

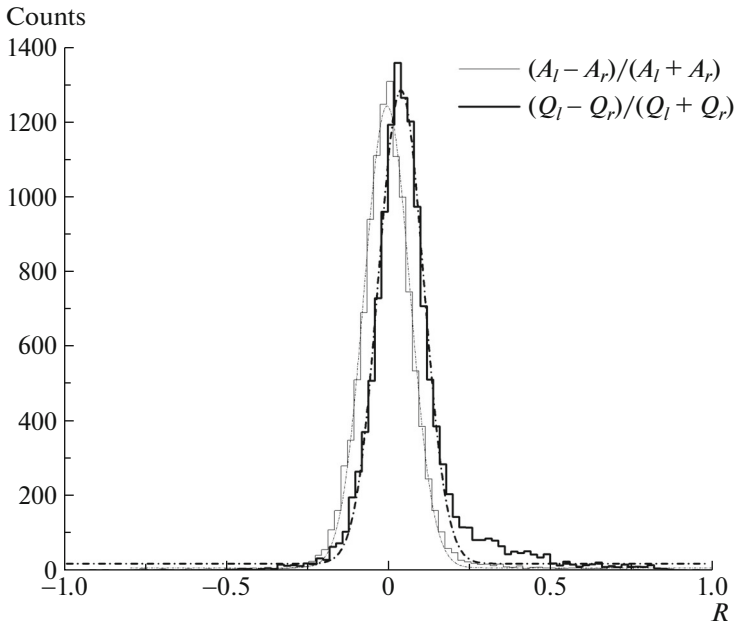

Fig. 4. The distributions of the ratio R for positron beam position in the center of tested prototype detector. Full thin and thick lines match the amplitude and charge measurements respectively, dash–dot lines—to corresponding Gaussian approximations.

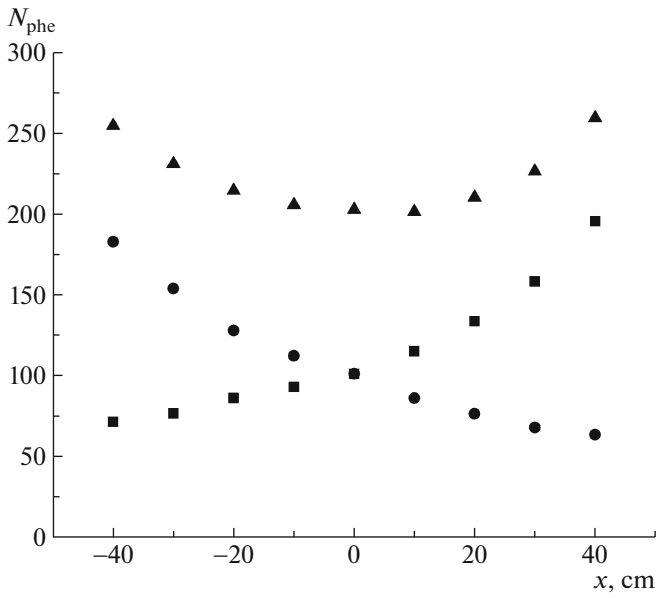

Fig. 5. Average total number of photoelectrons registered per incident positron at each end of the prototype detector strip as a function of the beam impact position relative to the detector centre. The squares present data for the left strip end, circles—for the right end, triangles—for left and right end sum. Error bars are smaller than the points on the plot.

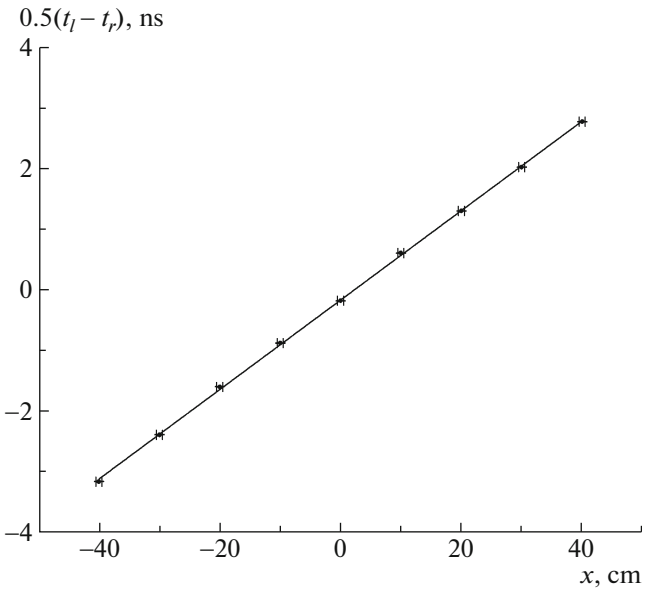

Fig. 6. Straight line fit to the semi-resultant of times of scintillation light arriving at the strip ends at different beam positions relative to the detector centre. The inverse slope of the fit gives the effective scintillation light velocity $v = 13.1 \pm 0.1$ cm ns^{-1} in the prototype detector strip.

amplified and shaped signals are fed into the four-channel CFD (ORTEC Model 935). The CFD outputs are connected through the set of delay lines to the coincidence the logic unit (CAEN Model N405) which generates the reference start time pulse $M = M1 \wedge M2 \wedge M3 \wedge M4$ for the positrons' registration. Two quad scalers are used for counting $M1$–$M4$ and M pulses. The beam monitor time resolution

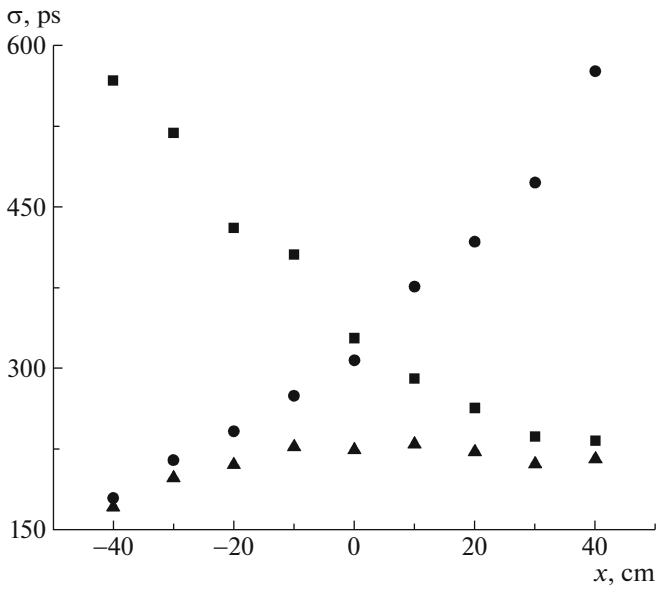

Fig. 7. The time resolution measured at each end of the prototype detector strip as a function of the beam impact position relative to the detector centre. The squares are data for the left strip end, circles—for the right end, triangles—combined time resolution σ_{lr} at both ends obtained as $1/1\sigma_{lr}^2 = 1/\sigma_l^2 + 1/\sigma_r^2$. Error bars are smaller than the points on the plot.

was measured as 104 ± 2 ps. The beam monitor functional diagram is shown in Fig. 2.

3. STUDIES OF THE PROTOTYPE DETECTOR

To characterize the prototype detector, the measurements of the following parameters defined its time resolution were carried out: attenuation length, photostatistics, effective light velocity and intrinsic time resolution. The statistics at each data point is about 10^4 for all results presented. The measurements of the absolute detection efficiency require much greater beam intensity to reach suitable accuracy in a reasonable accelerator time than the defined above secondary positron beam intensity and are in preparation now at the primary beam of synchrotron C-25P "PAKHRA".

3.1. Attenuation Length

Assuming that the light attenuation can be approximated by a single exponential function, we can formulate the following relations for light attenuation in the scintillator:

$$A_l(x) = C_l \exp\left(-\frac{\frac{L}{2} - x}{\lambda}\right), \qquad (1)$$

$$A_r(x) = C_r \exp\left(-\frac{\frac{L}{2} + x}{\lambda}\right).$$

Here, L and λ represent the length and attenuation length of the scintillator; x denotes the hit position from the center of the scintillator; A_l and A_r are measured signal amplitudes from the left and right scintillator ends. Appropriate proportionality constants C_l and C_r depend on the stopping power of charged particles, light attenuation due to optical couplings between the scintillator and photosensor block, etc. Taking the ratio of the above two equations, the attenuation length λ can be expressed as:

$$0.5 \ln \frac{A_l}{A_r} = \frac{1}{\lambda} x + 0.5 \ln \frac{C_l}{C_r}, \qquad (2)$$

which is a straight-line equation of the variable $y(x) = 0.5 \ln (A_l/A_r)$ with the inverse slope parameter of λ. The measured A_l/A_r distributions for different x positions were fitted with a Gaussian. The mean values of the Gaussian distributions for the prototype detector are plotted in Fig. 3. A least-square ?t to a straight line gives $\lambda = 91 \pm 1$ cm, which is approximately one fourth of the attenuation length for a bulk scintillator [8].

3.2. Photostatistics

The measurement of charge or amplitude of the detector output signals allows estimating the lower limit of the total number of photoelectrons produced by the particles into the scintillator. Assuming g_i—gain and ε_i—efficiency of the photosensor blocks ($i = l$, r—left and right counter sides' indexes) are equalized, i.e. $g_i \times \varepsilon_i = \text{const}$; $N_{\text{phe}} = N_{\text{phe}}^l + N_{\text{phe}}^r$ is the total number of photoelectrons collected at both sides of the counter; Q_i and A_i are the measured charge and amplitude of signals and $Q_i = \text{const} \times A_i = g_i \varepsilon_i N_{\text{phe}}^i$ one can write:

$$R = \frac{Q_l - Q_r}{Q_l + Q_r} = \frac{A_l - A_r}{A_l + A_r} = \frac{N_{\text{phe}}^l - N_{\text{phe}}^r}{N_{\text{phe}}^l + N_{\text{phe}}^r} \qquad (3)$$
$$= \frac{N_{\text{phe}}^l - N_{\text{phe}}^r}{N_{\text{phe}}} = \frac{2N_{\text{phe}}^l}{N_{\text{phe}}} - 1.$$

Supposing that N_{phe}^l follows a binomial distribution, N_{phe} and standard deviation on R are given by:

$$\sigma_R = \frac{2}{N_{\text{phe}}} \sqrt{N_{\text{phe}} p (1-p)} = \frac{1}{\sqrt{N_{\text{phe}}}}, \qquad (4)$$
$$p = \frac{1}{2}, \quad \text{and} \quad N_{\text{phe}} = \frac{1}{\sigma_R^2}.$$

In Fig. 4 the distributions of the ratio R for the positron beam impact in the center of the tested prototype detector are shown. The corresponding total photoelectron numbers 203 ± 3 for amplitude measurements and 209 ± 6 for charge measurements match the statistical errors. In Fig. 5 the average photoelectron yield per incident positron is presented as a function of the beam position.

3.3. Timing Measurements

For studying the prototype detector timing properties the distributions of three time intervals for the set of positron beam positions along the strip were analyzed: $(t_l - t_M)$, $(t_r - t_M)$, and $(t_l - t_r)$. Here t_l and t_r are the measured signal arriving times from each end of the strip and t_M is the trigger reference signal M moment from the positron beam monitor. The measured distributions were fitted by the Gaussian function and the resulting mean values and standard deviations were used for further analysis.

The positron position x along the strip is determined as $x = 0.5v\,(t_l - t_r)$. The effective speed of scintillation light propagation v along the strip is calculated by linear fitting of expression $0.5\,(t_l - t_r) = x/v$ as inverse value of the fit slope. The corresponding result is presented in Fig. 6. The time resolutions σ_l and σ_r for each end of the scintillator strip are shown in Fig. 7 together with combined resolution $\sigma_{lr} = \sigma_l\sigma_r/\sqrt{\sigma_l^2 + \sigma_r^2}$ as a function of the beam position along the strip relative to the strip centre. All resolutions shown represent the fitted Gaussian standard deviation of the corresponding distributions, corrected for the resolution of the beam monitor and uncertainty due to finite size of the positron beam ($\sim$1 cm). As expected, the time resolutions σ_l and σ_r worsen with the increase in distance of the beam position from respective SiPMs block. The combined time resolution is the worst ($\sim$230 ps) at the centre of the strip due to the less light collected by SiPMs.

4. CONCLUSION

The prototype detector on the base of $1280 \times 100 \times 10$ mm^3 BC-408 polyvinyltoluene scintillator strips with readout at both ends by photosensor blocks consisting of four SiPMs of the type SensL MicroFC60035-SMT was developed for carrying out a series of experiments in order to study amplitude, triggering and timing characteristics of the anticoincidence system of the GAMMA-400 gamma-ray telescope. The properties of the prototype are measured using 300-MeV/c secondary positron beam of the synchrotron C-25P "PAKHRA" of Lebedev Physical Institute. The intrinsic time resolution of the prototype detector is found to be not worse than 230 ps which is enough for reliable suppression of the backsplash events. The measured effective scintillation light velocity is 13.1 ± 0.1 cm ns^{-1}. The measured attenuation length is 91 ± 1 cm, which is one quarter of the corresponding length of a bulk scintillator. This value is about 1.5 times less than the one expected and can be explained by degradation of the scintillator strip (the microcracks net was disclosed on the scintillator surface after thorough inspection). For further improvement of the prototype parameters the defective strip was replaced, the number of SiPMs at each detector end was increased up to 8 instead of currently used 4 SiPMs and the new type of silicon photomultipliers SensL MicroFJ-60035-TSV with enhanced photon detection efficiency and lower dark count rate were employed for obtaining the better photoelectron statistics and time resolution. The "fast" SiPM outputs were used as a source of signal for timing measurements too.

ACKNOWLEDGMENTS

The authors thank for the support from National Research Nuclear University MEPhI in the framework of the Russian Academic Excellence Project (contract no. 02.a03.21.0005, 27.08.2013).

REFERENCES

1. N. P. Topchiev, A. M. Galper, V. Bonvicini, O. Adriani, R. L. Aptekar, I. V. Arkhangelskaja, A. I. Arkhangelskiy, L. Bergstrom, E. Berti, G. Bigongiari, S. G. Bobkov, E. A. Bogomolov, M. Boezio, M. Bongi, S. Bonechi, S. Bottai, et al., Bull. Russ. Acad. Sci. Phys. **79**, 417 (2015).
2. A. M. Galper, N. P. Topchiev, and Yu. T. Yurkin, Astron. Rep. **62**, 882 (2018).
3. A. S. Syrov, V. V. Smirnov, V. N. Sokolov, G. S. Iodko, V. V. Mischihin, V. N. Kosobokov, M. A. Shatsky, and D. A. Dobrynin, Cosmonaut. Rocket Engin. **3**, 58 (2015).
4. A. A. Moiseev, R. C. Hartman, J. F. Ormes, D. J. Thompson, M. J. Amato, T. E. Johnson, K. N. Segal, and D. A. Sheppard, Astropart. Phys. **27**, 339 (2007).
5. M. D. Kheymits, A. M. Galper, I. V. Arkhangelskaja, A. I. Arkhangelskiy, Yu. V. Gusakov, V. G. Zverev, V. V. Kadilin, V. A. Kaplin, A. A. Leonov, P. Yu. Naumov, M. F. Runtso, S. I. Suchkov, N. P. Topchiev, and Yu. T. Yurkin, Instrum. Exp. Tech. **59**, 508 (2016).
6. I. V. Arkhangelskaja, A. I. Arkhangelskiy, E. N. Chasovikov, A. M. Galper, M. D. Kheymits, A. E. Murchenko, and Y. T. Yurkin, J. Phys.: Conf. Ser. **675**, 032015 (2016).
7. K. O'Neill and C. Jackson, Nucl. Instrum. Methods A **787**, 169 (2015).
8. Organic Scintillation Materials and Assemblies, Saint Gobain Crystals (Web document accessed June 2019). https://www.crystals.saint-gobain.com/sites/imdf.crystals.com/files/documents/organics-plastic-scintillators.pdf.